The effect of boiling off of neutrons is to produce the modified distribution of nuclei shown in Table II. Of these elements, two at least are positron emitters and so more easily detected. It is possible that there are others among the unknown isotopes which are positron active. The activity which can be collected is somewhat marginal. Consider for example the collected activity to be expected for the positron emitter $_{69}Tm^{166}$; assume 10^{-10} of the bomb is collected. Then the collected radio activity of $_{69}Tm^{166}$ produces one decay per minute.

The yield of fusion elements is proportional to

$$(\sigma/v_{\rm rel})\theta^3\epsilon^2(V/T),$$

where θ is the electron temperature, ϵ is the efficiency, and V is the reaction volume. In the case of the hydrogen bomb both the volume and the electron temperature are expected to be larger than in an ordinary fission explosion. The hydrogen bomb, therefore, offers an opportunity for an increased yield of nuclear species produced by fission fragment fusion.

In view of the recently developed theories of supernovae explosion,[2] involving production of Cf^{254} and other fissile nuclei, it may be important to consider the subsequent fusion of fission fragments in supernovae. If this process is sufficiently important, it may affect the astrophysical abundances of elements in the region of platinum.

[2] G. R. Burbidge, F. Hoyle, E. M. Burbidge, R. F. Christy, and W. A. Fowler, Phys. Rev. **103**, 1143 (1956).

PHYSICAL REVIEW VOLUME 129, NUMBER 2 15 JANUARY 1963

Elastic and Inelastic Scattering of 31.1-MeV Protons by Carbon-12*

J. KIRK DICKENS,† DAVID A. HANER, AND CHARLES N. WADDELL
University of Southern California, Los Angeles, California
(Received 17 August 1962)

The angular distributions of 31.1-MeV protons scattered by the ground state and the 4.4-, 7.7-, 9.6-, 12.7-, 14.0-, 15.1-, and 16.1-MeV excited states have been measured. The differential cross sections for the elastic scattering have been analyzed using the diffuse-surface optical model of the nucleus for a wide range of parameters. This analysis indicates that at this energy the best fit requires a potential characterized by volume, as well as surface, absorption. The angular distributions of the inelastically scattered protons are peaked forward and have been compared to predictions of direct interaction theories.

I. INTRODUCTION

THE recent optical-model analysis by Nodvik, Duke, and Melkanoff of the elastic scattering of 12- to 19-MeV protons by carbon has shown that excellent fits to the experimental data can be obtained for a light nucleus.[1] The most striking features of the results are the thin absorptive shell and the absence of volume absorption that characterize the optical-model potential over most of the studied energy range. However, for $17.8 \leqslant E_p \leqslant 18.9$ MeV the analysis indicates either a broadening of the absorptive part of the potential or the necessity for including volume absorption, or, possibly, both.

This work also emphasizes the need for accurate experimental data at small energy intervals over a sizeable range of incident energies. As the first step in an experimental program to extend the measurements of elastic scattering from carbon to the 20- to 30-MeV range, the results obtained at the full energy of the U.S.C. Linac are presented in this paper.

The angular distributions of protons inelastically scattered from various excited states of C^{12} were measured simultaneously. These differential cross sections are peaked forward and are not symmetric about 90°, indicating the presence of a direct interaction mechanism rather than the formation of a compound nucleus.[2] The measured angular distributions are compared to the predictions of several existing direct interaction theories.[3–5]

II. EXPERIMENTAL DETAILS

A. General

The University of Southern California proton linear accelerator has been described by Alvarez *et al.*,[6] and

* Work supported in part by the U. S. Atomic Energy Commission.

† Present address: Oak Ridge National Laboratory, Oak Ridge, Tennessee.

[1] J. S. Nodvik, C. B. Duke, and M. A. Melkanoff, Phys. Rev. **125**, 975 (1962).

[2] W. Tobocman, *Theory of Direct Interactions* (Oxford University Press, New York, 1961).

[3] N. Austern, S. T. Butler, and H. McManus, Phys. Rev. **92**, 350 (1953).

[4] J. S. Blair, Phys. Rev. **115**, 928 (1959).

[5] J. D. Templin, thesis, University of California at Los Angeles, 1961 (unpublished).

[6] L. W. Alvarez, H. Bradner, J. V. Franck, H. Gordon, J. D.

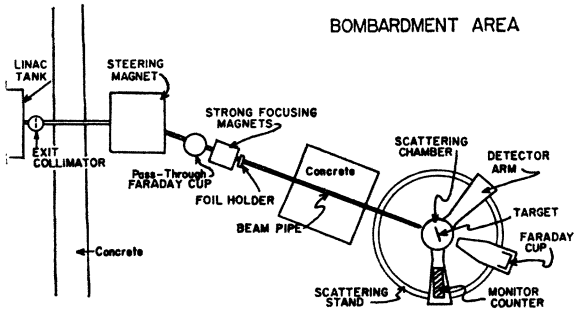

FIG. 1. The experimental arrangement for proton-scattering experiments.

the main characteristics of the beam are as follows: nominal energy, 31.5 MeV; estimated energy spread, less than ± 200 keV; approximate diameter of emerging beam, 1 cm; angular divergence, 10^{-3} rad; repetition rate, 15 pps; pulse length, 500 μsec; output current, $\sim 3\times 10^{-7}$ A, average, and ~ 60 μA, peak; duty cycle, approximately 0.75%.

The equipment in the bombardment area is shown in Fig. 1. The intensity of the proton beam is varied by the adjustable exit collimators, and the beam is deflected through a 10° angle, focused on the target by the strong-focusing quadrupole magnets, and collected in a Faraday cup.

B. Scattering Stand

A general purpose scattering apparatus, very similar to the one described by Brussel and Williams[7] was used in this study. The two arms of the 8-ft-diam scattering stand easily support a half ton of shielding, and can be rotated through 360° with a positioning accuracy of $\pm 0.02°$. The targets are contained in a 14-in-diam evacuated scattering chamber that has a thin Mylar-covered window 2 in. high and 320° in aperture. The five-position target ladder can be remotely positioned to ± 0.03 in. and to 0.25° with respect to the beam line.

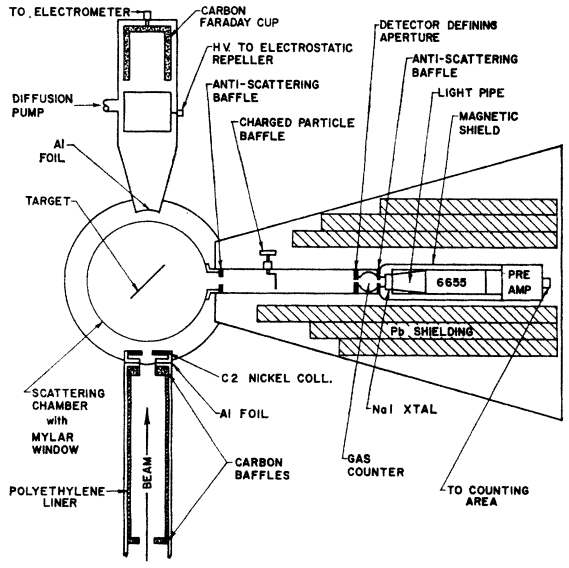

FIG. 2. A detailed view (not to scale) of the proton-scattering system.

As shown in Fig. 2, this chamber is connected to the detector assembly, rather than to the beam pipe (as described in reference 7). This has the following advantages: (a) The scattered protons travel in vacuum from the target to the counters, resulting in minimum energy degradation and multiple scattering; and (b) the scattering chamber rotates with the counter arm, reducing the effects of radiation damage to the Mylar window.

C. Beam Integration

The beam was monitored by a carbon Faraday cup 6 in. deep and 6 in. in diameter placed approximately 3 ft from the target. Carbon was chosen because its low neutron production produced minimum background.[8] The entrance foil to the Faraday cup was about 2 ft from the cup and an electrostatic repeller electrode was placed between the foil and the cup. The collected charge was integrated using a calibrated low-leakage polyethylene capacitor and the emf was measured with a 100% feedback electrometer.

The pressure in the Faraday cup housing was less than 10^{-4} mm of mercury. No effect upon beam collection, due to electrons ejected from the Faraday cup or the entrance foil, was seen upon application of a negative potential to the repeller electrode; however, an effect as large as 1% could have been present and not detected. The loss of beam due to multiple scattering in windows and the target was calculated to be less than 0.05%.[9]

A monitor counter was set up (see Fig. 1) and calibrated with the Faraday cup to a 1% statistical ac-

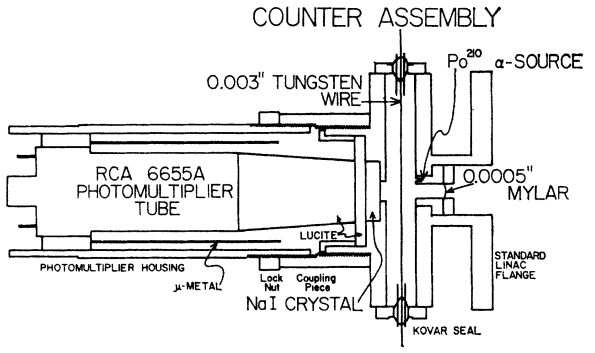

FIG. 3. A detailed view of the counter telescope. The NaI(Tl) crystal is placed inside the gas counter.

Gow, L. C. Marshall, F. Oppenheimer, W. K. H. Panofsky, C. Richman, and J. R. Woodyard. Rev. Sci. Instr. **26**, 111 (1955).

[7] M. K. Brussel and J. H. Williams, Phys. Rev. **114**, 525 (1959).

[8] Y. K. Tai, G. P. Millburn, S. N. Kaplan, and B. J. Moyer, Phys. Rev. **109**, 2086 (1958).

[9] H. Bichsel, University of Southern California Nuclear Physics Laboratory, Technical Report No. 2, Los Angeles, 1961 (unpublished).

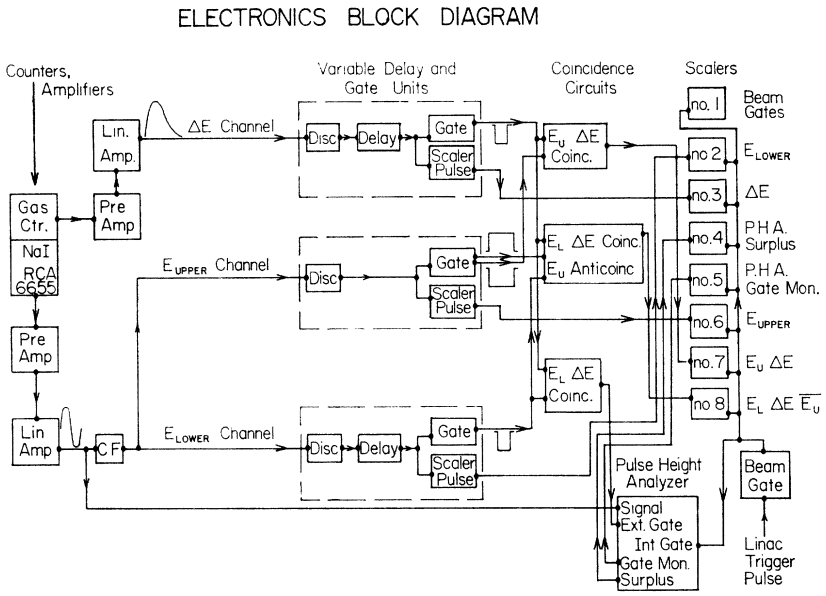

FIG. 4. Block diagram of the electronic equipiment.

curacy. It was used as the beam monitor for laboratory angles less than 22 deg.

D. Detector Assembly

The scattering chamber, target, proton pipe, and counter assembly are shown in more detail in Fig. 2. The size of the target beam spot is determined by the nickel collimator C-2. All collimators are made of nickel because nickel has a low neutron production[8] and introduces the smallest slit scattering effect.[10] The positions and sizes of the collimators and the diameter of the proton pipe were chosen to eliminate wall scattering effects. The angular breadth of scattered protons accepted by the detector defining aperture is 0.45 deg.

The protons were detected by a counter telescope consisting of a proportional counter and a NaI(Tl) scintillation counter as shown in Fig. 3. The proportional counter is similar to one described by Igo and Eisberg.[11] It was filled to $1\frac{1}{2}$ atm. with a 91% argon, 9% methane mixture. A weak Po^{210} alpha source was included so the counter's operation could be checked at any time. The performance of the proportional counter was checked by measuring the pulse-height distribution obtained for 30-MeV protons; the expected Landau distribution was obtained.[11]

The scintillation counter consisted of a $\frac{1}{4}$-in.-thick NaI(Tl) crystal optically coupled to an RCA 6655A photomultiplier tube. Since the crystal was placed inside the gas counter, a transparent vacuum seal was required as part of the optical coupling. This construction did not seem to affect the resolution. The potential distribution between the photocathode, grid, and first dynode was held constant by using a battery supply, and the grid potential was adjusted to maximize photoelectron collection. Thus, changing the high voltage applied to the dynode structure to change the gain did not affect the photoelectron collection.

E. Electronics

The general functions of the electronics were (a) to pulse-height analyze all pulses from the NaI crystal coincident with appropriate pulses from the proportional counter, (b) to monitor the operation of the equipment while the experiment was in progress, and (c) to measure the counting losses during the experiment.

The block diagram of the electronics is shown in Fig. 4. The discriminator in the ΔE channel was adjusted to trigger on all proportional counter pulses produced by elastically scattered protons. The E_{upper} discriminator was adjusted to trigger on all NaI pulses produced by elastically scattered protons, and the E_{lower} discriminator was adjusted to trigger on pulses from protons inelastically scattered from C^{12} levels of excitation less than $\sim$18 MeV.

In normal operation the output of the $E_L\Delta E$ coincidence circuit was used to gate the Penco PA-4 pulse-height analyzer. The outputs of the other coincidence circuits and the "singles" counts from the three discriminators were monitored by scalers. The pulse-height analyzer and each scaler were gated by the "beam gate" to count only during the beam pulse.

Determining the counting losses was very important, since the accelerator duty cycle is $\sim$1% and an amplitude-to-time conversion pulse-height analyzer was used. The average singles counting rate of each counter

[10] E. J. Burge and D. A. Smith, in *Proceedings of the Rutherford Jubilee International Conference, Manchester, 1961*, edited by J. B. Berks (Academic Press Inc., New York, 1961), Abstract C8/25; and (private communication).

[11] G. J. Igo, D. D. Clark, and R. M. Eisberg, Phys. Rev. **89**, 879 (1953).

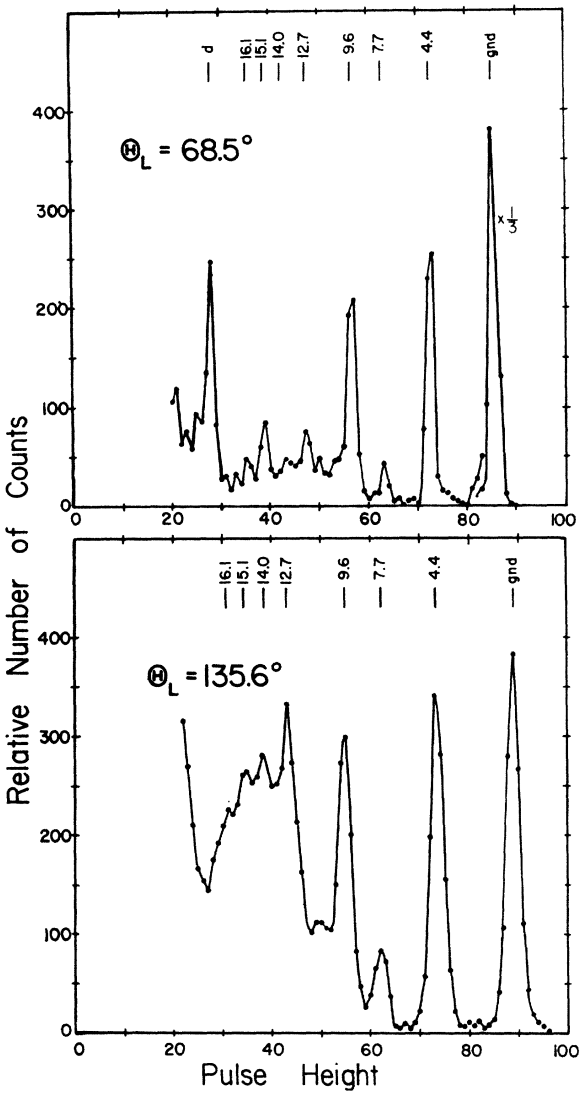

FIG. 5. Scintillation counter coincidence-gated spectrum obtained at 68.5° and 135.6°. The peaks corresponding to protons scattered from known levels in C^{12} and the peak corresponding to deuterons from the reaction $C^{12}(p,d)C^{11}$ are indicated.

was restricted to $\leqslant$ one count per beam pulse, and at this counting rate the counting losses in the scalers were $\sim 0.2\%$. Scaler No. 6, which monitored the number of elastically scattered protons, recorded no background counts. Comparison of the number of counts recorded in scaler No. 6 with those in the elastic peak showed that the counting losses in the pulse-height analyzer averaged 2% and were never higher than 4%.

III. EXPERIMENTAL RESULTS

A. Observed Spectra

Data were taken at 2- to 10-deg intervals between laboratory angles of 9 and 157 deg. Throughout most of this range, the laboratory angles were chosen to give integral center-of-mass angles for the elastic peak. A minimum of 1100 counts was obtained in the elastic peak at each angle.

Figure 5 shows spectra obtained at 68.5° and 135.6°. The peaks corresponding to protons scattered from known levels in C^{12} and the peak corresponding to ground-state deuterons from the reaction $C^{12}(p,d)C^{11}$ are indicated in this figure. In addition, the figure shows the continuum of protons from the reaction $C^{12}(p,p')3\alpha$ having a Q value of -7.2 MeV.[12,13]

B. Reduction of Data

Determining the net number of counts corresponding to elastically scattered protons was relatively free from ambiguity. The resolution of the scintillation counter and related electronics, typically $2\frac{1}{2}$ to 3%, allowed a clear separation of the elastic peak from the 4.4-MeV level peak, and no background in the elastic peak was observed.

Three corrections were applied to the yield recorded by the pulse-height analyzer. (a) The contribution to the yield from collimator penetration must be subtracted. An estimate based upon Burge's calculations[10] indicated a correction $\sim 1\%$ for a $\frac{1}{4}$-in. nickel collimator. To check this the collimator size was varied, and the experimental value agreed with the calculated value. (b) The effect of nuclear interactions of the protons entering the NaI crystal decreases the measured elastic cross section. The correction for this effect is $\sim 1\%$.[14] Thus, fortuitously, these two corrections cancelled each other. (c) To correct for counting losses in the pulse-height analyzer the elastic yield obtained in the pulse-height analyzer was normalized to that obtained in scaler No. 6 (See Sec. II E for discussion).

For the inelastic levels the contribution to the counting rates from slit-edge penetration and crystal reactions of the elastically scattered protons was subtracted from the observed yields. In all cases this subtraction was less than the statistical accuracy of the data.

For scattering by the 4.4-MeV level no further corrections were made. However, for scattering by the remaining levels, the number of protons in the continuum had to be estimated to obtain the net number of counts in a given peak. All spectra were normalized to Q value in order to obtain a more accurate determination of the yield. The total number of counts and the estimated number of subtracted counts for each level were obtained from the normalized spectra.

Once the total numbers of counts and estimated subtraction counts were obtained, calculation of the cross section was performed by the University of Southern California Honeywell 800 computer. The computer pro-

[12] F. Ajzenberg-Selove and T. Lauritsen, Nucl. Phys. **11**, 1 (1959).

[13] H. B. Knowles, University of California Radiation Laboratory Report UCRL-3753, 1957 (unpublished).

[14] L. H. Johnston and D. A. Swenson, Phys. Rev. **111**, 212 (1958).

TABLE I. Differential cross sections for the elastic scattering of 31.1-MeV protons by C^{12}.

θ_{lab} (deg)	$(d\sigma/d\omega)_{lab}$ (mb/sr)	$\theta_{c.m.}$ (deg)	$(d\sigma/d\omega)_{c.m.}$ (mb/sr)		Relative % error	Absolute % error
9.2	1,239	10.0	1,057	±38	3.6	4.5
11.1	994	12.0	848	31	3.6	4.5
13.9	889	15.0	761	18	2.0	4.5
18.5	685	20.0	588	22	3.7	4.6
23.1	527	25.0	455	11	2.2	4.5
25.4	452	27.4	391	12	2.7	4.2
27.8	357	30.0	309	10	3.2	4.2
32.4	205	35.0	179	6	3.2	4.2
37.1	111.5	40.0	98.1	3.2	3.3	4.2
41.8	56.0	45.0	49.7	1.7	3.5	4.4
42.5	48.4	45.8	43.0	1.5	3.4	4.3
45.0	33.3	48.4	29.7	0.9	2.3	4.2
46.5	28.3	50.0	25.3	1.0	3.9	4.7
48.4	22.4	52.0	20.1	0.5	2.1	4.3
51.3	16.7	55.0	15.1	0.6	4.3	5.0
54.1	16.2	58.0	14.8	0.4	2.5	4.4
57.0	16.2	61.0	14.9	0.3	2.3	4.2
60.0	16.1	64.1	14.8	0.4	2.5	4.3
62.7	16.5	67.0	15.4	0.4	2.5	4.4
65.6	15.4	70.0	14.4	0.4	2.6	4.4
68.5	14.6	73.0	13.8	0.4	3.1	4.4
71.4	13.0	76.0	12.4	0.4	2.9	4.5
74.4	12.27	79.0	11.77	0.38	3.2	4.4
77.3	10.19	82.0	9.85	0.29	3.0	4.2
80.3	8.76	85.0	8.55	0.33	3.9	4.7
83.2	6.78	88.0	6.67	0.27	4.1	4.8
90.0	4.49	94.8	4.51	0.17	3.8	4.6
95.2	3.21	100.0	3.27	0.14	4.4	5.1
99.3	2.61	104.0	2.69	0.13	5.0	7.1
105.4	1.79	110.0	1.88	0.06	3.5	4.6
109.5	1.50	114.0	1.58	0.07	5.1	7.2
115.7	1.085	120.0	1.173	0.024	2.0	3.5
120.9	0.905	125.0	0.991	0.024	2.4	4.0
126.0	0.747	129.9	0.827	0.018	2.2	3.8
128.2	0.705	132.0	0.787	0.015	2.0	3.6
130.3	0.662	134.0	0.742	0.017	2.3	3.7
132.5	0.644	136.0	0.724	0.016	2.2	3.6
135.6	0.661	139.0	0.750	0.016	2.1	3.4
138.8	0.666	142.0	0.761	0.017	2.2	3.6
142.0	0.655	145.0	0.752	0.017	2.2	3.6
145.3	0.652	148.0	0.753	0.023	3.0	4.1
146.5	0.655	149.2	0.759	0.023	3.0	4.1
148.4	0.648	151.0	0.752	0.017	2.2	3.6
151.7	0.624	154.0	0.728	0.017	2.3	3.6
155.0	0.554	157.0	0.649	0.016	2.5	3.8
157.0	0.539	158.9	0.634	0.019	3.9	4.1
158.2	0.507	160.0	0.596	0.026	5.2	6.9

gram first determined the angular distribution of the estimated counts of continuum protons at the energy of a given proton group, and then fitted a second-order polynomial to this distribution by a least-squares analysis. Values obtained from this curve were used for the actual subtraction. Quoted errors indicate the estimate of the reliability of this computation. The computer also converted laboratory angles and cross sections into the center of mass using standard nonrelativistic equations.

C. Errors

The contributions to the assigned error were divided into statistical and nonstatistical errors for computational purposes. The standard deviation was determined by the total number of counts and the number of subtraction counts. The nonstatistical errors were further divided into relative errors (affecting only the shape of the differential cross section curve), and absolute errors (primarily affecting the absolute normalization). Errors were assigned for each run; the average relative error was ~2%, and the average absolute error was ~4%. In the computer program the net nonstatistical relative and absolute errors were quadratically combined with the computed statistical error to provide the total relative and absolute error assigned to the differential cross section being calculated.

IV. RESULTS AND DISCUSSION

A. Elastic Scattering

The measured elastic differential cross sections and associated errors are presented in Table I. For angles less than ~55° these data agree with previously re-

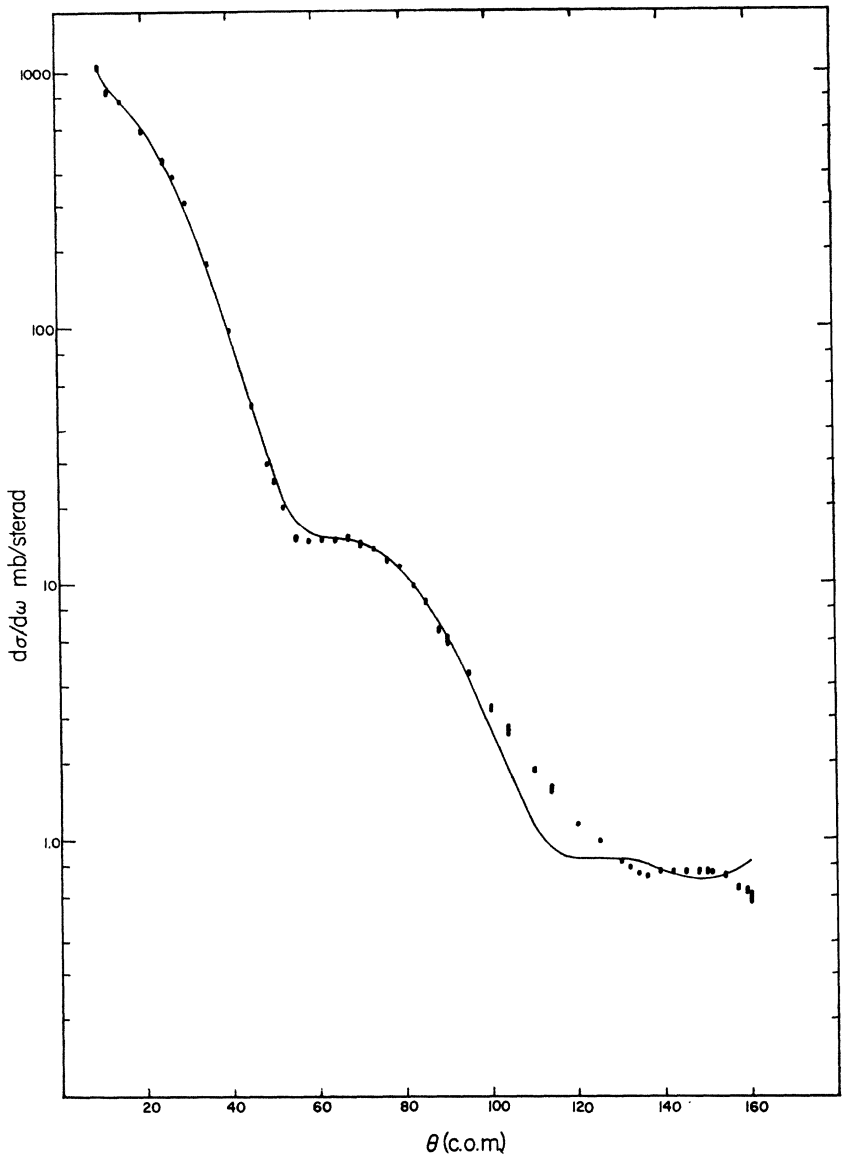

FIG. 6. The angular distribution of 31.1-MeV proton elastic scattering from C^{12}. The solid curve is the optimum fit obtained using the diffuse-surface optical model of the nucleus. The parameters for this fit are given in the text.

ported cross sections.[15–18] For angles greater than $\sim 75°$ they agree with Wright's data within his assigned errors of $\sim 10\%$, but they depart significantly from the more accurate measurements of Hecht. Because of this discrepancy, these measurements were repeated several times over a period of some months with slightly differing experimental arrangements, and the results were reproducible. Part, or all, of the lack of agreement may be due to the difference in reported bombarding energies.

The data were analyzed with the diffuse-surface optical model of the nucleus using the methods discussed by Nodvik, Duke, and Melkanoff.[1] The potential used is

$$V_{\text{Opt}} = -Vf(r) - iW(r) + V_{\text{Coul}} + V_{\text{SO}}.$$

In this equation the Wood-Saxon form factor is used for $f(r)$;

$$f(r) = [1+\exp(r-R)/a]^{-1},$$

where $R = R_0 A^{1/3}$. The form of $W(r)$ used in this analysis is

$$W(r) = W_1 \exp[-(r-R)^2/b^2] + W[1+\exp\{(r-R)/0.69b\}]^{-1},$$

where the first term corresponds to surface absorption and the second term corresponds to volume absorption.[1] V_{Coul} is the Coulomb potential corresponding to a uniformly charged sphere of radius R. A real spin-orbit

[15] R. Britten, Phys. Rev. **88**, 283 (1952).
[16] B. T. Wright, University of California Radiation Laboratory Report UCRL-2422, 1953 (unpublished).
[17] G. J. Hecht, University of California Radiation Laboratory Report UCRL-2969, 1955 (unpublished).
[18] B. B. Kinsey and T. Stone, Phys. Rev. **103**, 975 (1956).

TABLE II. Differential cross sections for the inelastic scattering of 31.1-MeV protons by the 4.43-MeV level of C^{12}.

θ_{lab} (deg)	$(d\sigma/d\omega)_{lab}$ (mb/sr)	$\theta_{c.m.}$ (deg)	$(d\sigma/d\omega)_{c.m.}$ (mb/sr)		Relative % error	Absolute % error
9.2	29.7	10.1	25.0	±3.0	12.0	12.7
11.1	26.7	12.1	22.5	1.8	8.1	8.9
13.9	29.0	15.1	24.5	1.7	7.0	7.6
18.5	23.8	20.1	20.1	2.4	12.0	12.7
23.1	24.7	25.2	21.0	3.2	15.0	15.5
25.4	23.8	27.6	20.3	1.1	5.5	7.4
27.8	22.2	30.2	19.0	1.7	8.9	9.2
32.4	18.3	35.2	15.8	0.8	5.0	5.6
37.1	16.7	40.3	14.5	0.6	4.4	5.2
41.8	14.03	45.3	12.31	0.57	4.6	5.3
42.5	13.32	46.0	11.72	0.51	4.4	5.1
45.0	12.14	48.7	10.82	0.35	3.2	4.5
46.5	11.52	50.3	10.23	0.50	4.9	5.6
48.4	9.53	52.3	8.50	0.33	3.9	4.9
51.3	8.94	55.3	8.02	0.41	5.1	5.8
54.1	6.67	58.3	6.03	0.31	5.2	5.8
57.0	5.55	61.4	5.05	0.18	3.5	4.6
60.0	4.81	64.5	4.41	0.21	4.8	5.5
62.7	4.05	67.4	3.74	0.23	6.1	6.6
65.6	3.04	70.4	2.83	0.15	5.2	5.8
68.5	2.63	73.4	2.47	0.13	5.3	7.2
71.4	2.39	76.4	2.26	0.17	7.5	7.9
74.4	2.08	79.4	1.99	0.10	5.0	5.7
77.3	1.77	82.4	1.71	0.09	5.1	5.7
80.3	1.57	85.4	1.53	0.10	6.3	6.8
83.2	1.77	88.4	1.74	0.10	6.0	6.6
90.0	1.56	95.2	1.58	0.08	4.9	5.6
95.2	1.37	100.4	1.40	0.08	5.7	6.2
99.3	1.25	104.4	1.28	0.07	5.8	6.3
105.4	0.977	110.4	1.030	0.045	4.4	5.1
109.5	0.763	114.4	0.815	0.046	5.7	6.3
115.7	0.654	120.4	0.711	0.020	2.9	4.1
120.9	0.575	125.4	0.635	0.022	3.4	4.4
126.0	0.562	130.2	0.630	0.020	3.2	4.2
128.2	0.592	132.3	0.667	0.016	2.4	3.7
130.3	0.627	134.3	0.710	0.017	2.7	3.7
132.5	0.623	136.3	0.710	0.017	2.4	3.7
135.6	0.621	139.3	0.713	0.016	2.3	3.6
138.8	0.624	142.3	0.720	0.016	2.3	3.6
142.0	0.604	145.3	0.702	0.016	2.3	3.7
145.3	0.573	148.2	0.671	0.021	3.2	4.3
146.5	0.576	149.4	0.676	0.021	3.2	4.3
148.4	0.514	151.2	0.605	0.015	2.5	3.8
151.7	0.467	154.2	0.553	0.014	2.6	3.8
155.0	0.412	157.2	0.490	0.014	2.8	4.0
157.0	0.353	159.0	0.421	0.015	3.7	4.6

potential of the Thomas type was used;

$$V_{SO} = -V_S(\hbar/m_\pi c)^2(1/r)(df/dr)\boldsymbol{\sigma}\cdot\mathbf{l}.$$

A preliminary survey was made using the following grid: $R_0=1.0$, 1.1, and 1.2 F; $W=0$, 2, 4, and 6 MeV; and $b=0.5$, 1.0, and 1.5 F. At each grid point the program determined the values of V, W_1, a, and V_S which minimized χ^2.[19] The fits obtained with $b=0.5$ F were definitely inferior to those obtained using $b=1.0$ and 1.5 F. The fits obtained with $b=1.0$ F have somewhat smaller χ^2 than those obtained with $b=1.5$ F. Further, the fits obtained with $R_0=1.0$ F were definitely inferior to those obtained with $R_0=1.1$ and 1.2 F.

[19] M. A. Melkanoff, J. S. Nodvik, D. S. Saxon, and D. G. Cantor, *A Fortran Program for Elastic Scattering Analysis with the Nuclear Optical Model* (University of California Press, Berkeley and Los Angeles, California, 1961).

The best fit obtained for the differential cross section curve is shown in Fig. 6. The parameters for this fit are: $R_0=1.1$ F, $V=54.3$ MeV, $a=0.64$ F, $W=4$ MeV, $W_1=6.49$ MeV, $b=1.0$ F, and $V_S=-3.7$ MeV. The predicted reaction cross section is 401 mb. These parameters—in particular those corresponding to the absorptive potential—show a definite change from $E_p \leqslant 19$ MeV to $E_p=31$ MeV. For $E_p \leqslant 19$ MeV the best fits were obtained with pure surface absorption, and a surface width of ~0.25 F.[1] At 31 MeV a combination of volume plus surface absorption is definitely required, and the width of the surface has increased to ~1.0 F.

B. Inelastic Scattering

(i) 4.4-MeV Level

The measured differential cross sections and associated errors for protons inelastically scattered from the

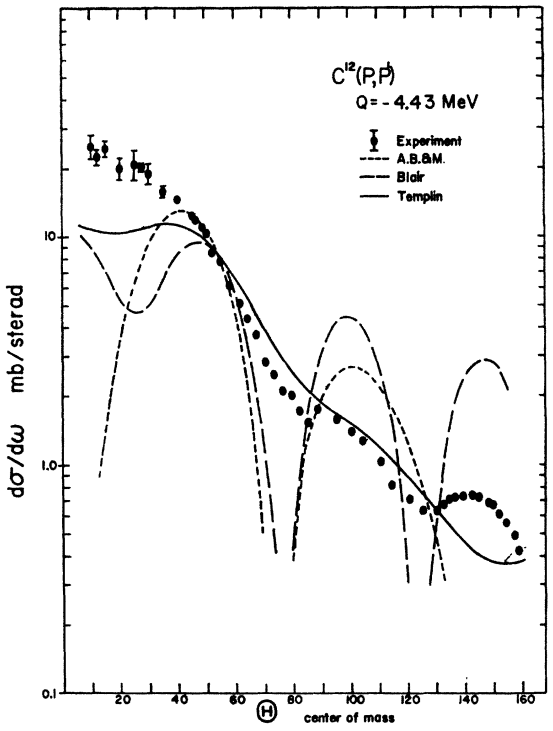

FIG. 7. The angular distribution of 31.1-MeV protons inelastically scattered from the 4.43-MeV level of C^{12}. The radius parameter for the $l=2$, ABM fit is $R_0=1.9$ F and for the $l=2$ Blair fit is $R_0=1.5$ F. The solid curve shows the result of a distorted-wave Born approximation calculation of J. Templin.

2^+ 4.4-MeV level of C^{12} are presented in Table II. As shown in Fig. 7 the angular distribution is strongly peaked forward, and a definite diffraction pattern is exhibited. Attempts were made to fit the data using the Austern, Butler, and McManus (ABM) theory,[3] the Blair theory,[4] and a direct-interaction distorted-wave Born approximation (DWB) theory developed by J. Templin.[5] These fits were computed for $l=2$ since the spin of this state is known; the best fits to the data are shown in Fig. 7. The radius parameter for the ABM fit is $R_0=1.9$ F, and for the Blair fit is $R_0=1.5$ F. The optical-model wave functions used in the DWB calculation were obtained from the analysis of the elastic scattering data.[20]

(ii) 7.7-MeV Level

The differential cross sections for protons inelastically scattered by the 0^+ 7.7-MeV level of C^{12} are shown in Fig. 8. The cross section for producing this level is small and the angular distribution shows forward peaking and exhibits a definite diffraction pattern. Theoretical fits to the data for $l=0$ are shown in Fig. 8. The theories reproduce the scattering by the 7.7-MeV level better than the scattering by the 4.4-MeV level. The radius parameter for the ABM fit is $R_0=1.6$ F, and for the Blair fit is $R_0=1.1$ F.

(iii) 9.6-MeV Level

The differential cross sections for protons inelastically scattered by the 9.6-MeV level of C^{12} are shown in Fig. 9. The angular distribution shows forward peaking, and a slight diffraction pattern is apparent. Since the spin and parity of this state are not definitely established (probably 1^- or 3^-),[12] an attempt was made to fit the data using several l values. The best fits obtained for $l=1$ and $l=3$ using the ABM and Blair theories are shown in Fig. 9. The radius parameter used for the $l=1$ ABM fit is $R_0=1.1$ F. For $l=3$, $R_0=1.9$ F for the ABM fit and $R_0=1.4$ F for the Blair fit.

A comparison of the theoretical curves with the experimental data indicates the difficulty in the assignment of spin and parity solely on the basis of these fits. Qualitatively, the Blair fit for $l=3$ fits the forward angles best and therefore suggests a spin and parity of 3^- in agreement with the suggested assignment of Carlson and Nelson.[21]

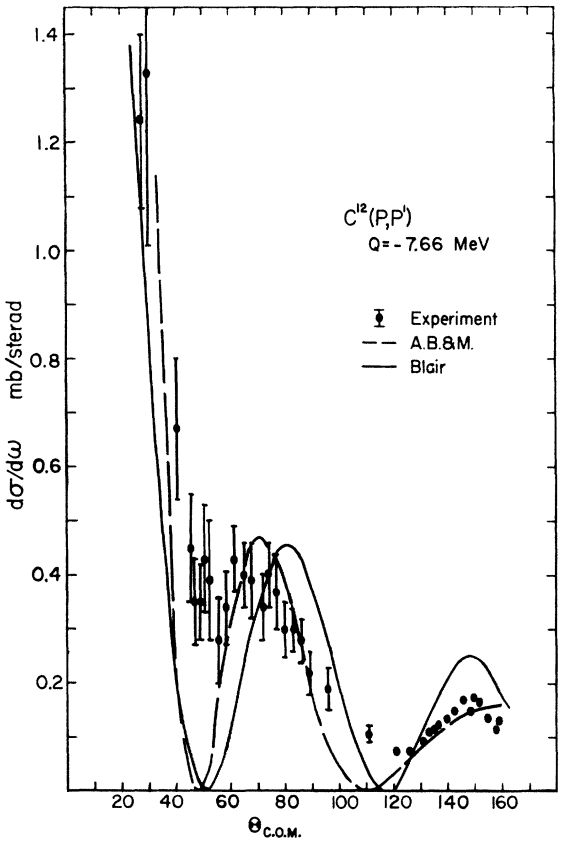

FIG. 8. The angular distribution of 31.1-MeV protons inelastically scattered from the 7.66-MeV level of C^{12}. The radius parameter for the $l=0$ ABM fit is $R_0=1.6$ F and for the $l=0$ Blair fit is $R_0=1.1$ F.

[20] The DWB calculation was done by J. Templin on the U.C.L.A. IBM 7090 computer.

[21] R. R. Carlson and E. B. Nelson, Bull. Am. Phys. Soc. 6, 341 (1961).

(iv) *12.7-MeV Level*

A larger uncertainty in cross section was introduced for levels of excitation energy greater than 9.6 MeV because the peaks were superimposed on the proton continuum (see Sec. III B for discussion). Angular distributions were computed only for levels which were definitely resolved at most angles (see Fig. 5). Because the errors for each point were large and almost entirely statistical, the data for two or three angles were combined to reduce these errors.

The differential cross sections for protons inelastically scattered from the 12.7-MeV level are shown in Fig. 10. The angular distribution shows typical forward peaking, and a definite diffraction pattern is exhibited. Since the spin and parity of this state are not definitely established an attempt was made to fit the data using several l values. Figure 10 shows the best ABM fits for $l=1$ and 2. For the $l=2$ fit the radius parameter is $R_0=1.6$ F, which is consistent with that used in fitting the lower levels. However, the $l=1$ fit has a radius parameter $R_0=1.3$ F, which is nearly equal to that used in fitting the 1^+ 15.1-MeV level (see Fig. 12). A fit for $l=3$ using a radius parameter $R_0=2.0$ F can be obtained, but fits for $l>3$ can be obtained only for unreasonably large radii. These results indicate that the spin of the 12.7-MeV level is probably $\leqslant 3$.

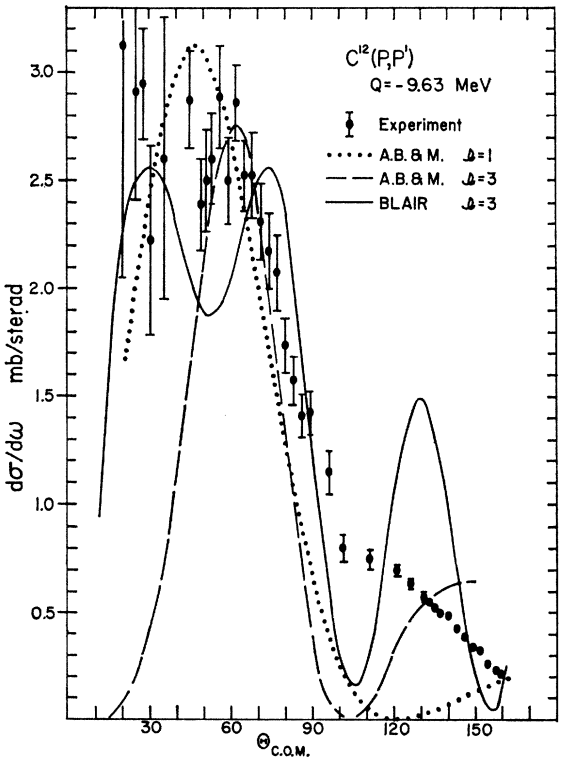

FIG. 9. The angular distribution of protons inelastically scattered from the 9.63-MeV level of C^{12}. The radius parameter for the $l=1$ ABM fit is $R_0=1.1$ F. For $l=3$, $R_0=1.9$ F for the ABM fit and $R_0=1.4$ F for the Blair fit.

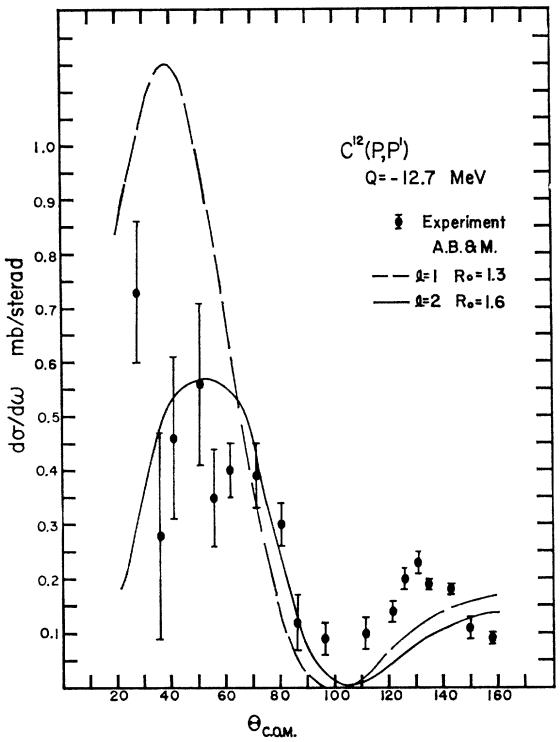

FIG. 10. The angular distribution of protons inelastically scattered from the 12.7-MeV level of C^{12}. The radius parameter for the $l=1$ ABM fit is $R_0=1.3$ F and for the $l=2$ ABM fit is $R_0=1.6$ F.

Despite the fact that the 12.7-MeV state is unstable by over 2 MeV against alpha emission to the 2^+ first excited state of Be^8 as well as to the 0^+ ground state, gamma-ray de-excitation has been observed.[22–24] In the study of the $B^{10}(He^3,p)C^{12}$ reaction, Almqvist *et al*, have found that this level de-excites $\sim 2\%$ of the time via gamma-ray emission, and they have made a tentative assignment of 1^+ to this state.[24]

The gamma-ray branching of the 12.7-MeV level produced in the $C^{12}(p,p')C^{12*}$ reaction can be estimated from the following data: (a) the integrated partial cross sections (see Table III) of 3.8 mb for the 12.7-MeV level excitation and 3.0 mb for the 15.1-MeV level excitation; (b) the determination by Hayward and Fuller that the gamma radiation width of the 15.1-MeV level is 69% of the total width[25]; and (c) the determination by Waddell that the thick target yield (for 31-MeV protons) of the ground-state gamma transition from the 12.7-MeV level is 8.2% of the total gamma yield of the 15.1-MeV level at 80°.[23] If the cascade transition via the 4.4-MeV level for the 12.7-MeV level is small in intensity compared to the ground-state transi-

[22] R. W. Kavanagh, thesis, California Institute of Technology, Pasadena, California, 1956 (unpublished).
[23] C. N. Waddell, University of California Radiation Laboratory Report UCRL-3901, 1957 (unpublished).
[24] E. Almqvist, D. A. Bromley, A. J. Ferguson, H. E. Gove, and A. E. Litherland, Phys. Rev. **114**, 1040 (1959).
[25] E. Hayward and E. G. Fuller, Phys. Rev. **106**, 991 (1957).

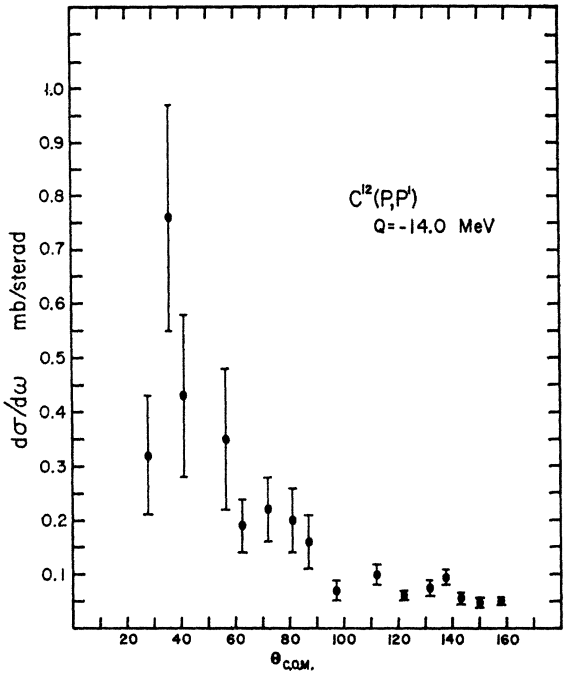

FIG. 11. The angular distribution of protons inelastically scattered from the 14.0-MeV level of C^{12}. No theoretical curves are shown as comparable fits could be obtained for values of l between 0 and 3.

tion (Almqvist *et al.*, place an upper limit of 20% for this ratio),[24] and if the excitation functions and gamma-ray angular distributions are assumed similar for the 12.7- and 15.1-MeV states, then the gamma branching of the 12.7-MeV level is calculated to be $4.5\pm1.5\%$. This is in reasonable agreement with the value of $2\pm1\%$ determined by Almqvist *et al.*, and, therefore, supports their assignment of 1^+ to this state.[24]

(v) *14.05-MeV Level*

The angular distribution of protons inelastically scattered by the 14.05-MeV level is shown in Fig. 11. Since the spin and parity of this state are not known, an attempt was made to fit the data using several l values. Because the angular distribution does not exhibit a diffraction pattern, no choice can be made between the various fits. Fits for $l>3$ can be obtained only for unreasonably large radii, and these results would seem to indicate that the spin of the 14.05-MeV level is probably $\leqslant 3$.

(vi) *15.1-MeV Level*

The differential cross sections for protons inelastically scattered from the 15.1-MeV level are shown in Fig. 12. This state is known to be a 1^+ state, and it is the first $T=1$ level in C^{12}.[12] The angular distribution is strongly peaked forward and a definite diffraction pattern is exhibited. An ABM fit for $l=1$, $R_0=1.35$ F is shown compared to the experimental data.

TABLE III. Partial cross sections for the inelastic scattering of 31.1-MeV protons by excited states of C^{12}.

Level energy (MeV)	$\sigma(p,p')$ (mb)
4.43	60.0 ± 2.4
7.66	4.7 ± 1.4
9.63	19.0 ± 1.6
12.7	$3.8^{+2.0}_{-1.0}$
14.0	$2.3^{+1.9}_{-0.9}$
15.1	$3.0^{+2.0}_{-1.0}$
16.1	$2.4^{+1.9}_{-0.9}$

(vii) *16.1-MeV Level*

The differential cross sections for protons inelastically scattered from the 16.1-MeV level are shown in Fig. 13. The spin and parity of this level is 2^+ and the isotopic spin is 1.[12] The scattering is peaked forward, but a definite diffraction pattern does not show up. The radius parameter for the $l=2$ ABM fit is $R_0=1.7$ F.

(viii) *Integrated Partial Cross Sections*

Presented in Table III are the integrated cross sections for the inelastic scattering of 31.1-MeV protons from the excited states of C^{12} discussed above. The in-

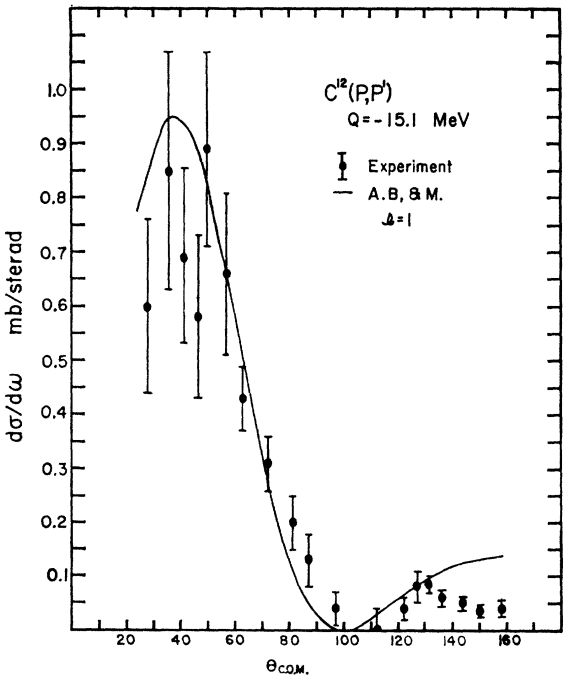

FIG. 12. The angular distribution of protons inelastically scattered from the 15.1-MeV, first $T=1$ level of C^{12}. The radius parameter for the $l=1$ ABM fit is $R_0=1.35$ F.

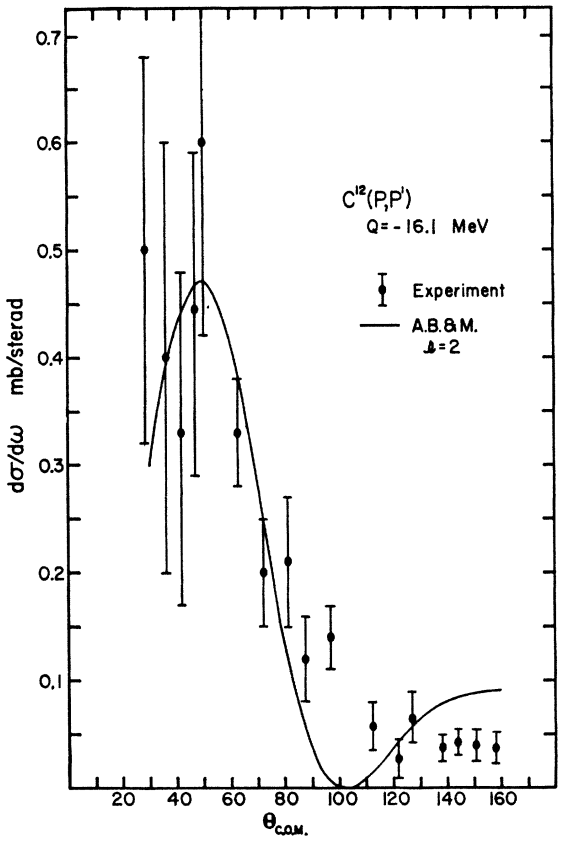

FIG. 13. The angular distribution of protons inelastically scattered from the 16.1-MeV level of C^{12}. The radius parameter for the $l=2$ ABM fit is $R_0=1.7$ F.

tegrals were obtained after extrapolating the measured angular distributions to 0° and 180°, and the quoted errors include the estimate of the reliability of this extrapolation.

V. SUMMARY

The analysis of the measured elastic differential cross sections with the diffuse-surface optical model of the nucleus indicates that the parameters are definitely different than those obtained for proton energies less than 19 MeV. For $E_p \lesssim 19$ MeV the best fits were obtained with pure surface absorption, and a surface width of ~ 0.25 F. At 31 MeV a combination of volume plus surface absorption is required, and the width of the surface has increased to ~ 1.0 F.

The angular distributions of inelastically scattered protons are peaked forward for all levels studied. Comparison of the measured angular distributions with those predicted by the ABM and Blair theories indicate that definite spin and parity assignments cannot be made solely on the basis of these analyses. Qualitatively, these analyses suggest that the spins of the 9.6-, 12.7-, and 14.05-MeV levels of C^{12} are $\lesssim 3$. An estimate of the gamma-ray branching ratio for the 12.7-MeV level supports the suggested assignment of 1^+ to this state.[24]

ACKNOWLEDGMENTS

We gratefully acknowledge the generous assistance of J. Sirois and the crew of the University of Southern California Linear Accelerator. We wish to thank Dr. J. Nodvik for his continuing interest and for permission to present the results of the optical-model analysis prior to publication. We are grateful to Dr. J. Templin of U.C.L.A. for providing us with the results of his calculations.